Comparison of signal-resonant and idler-resonant KTA-SROs

Fen Bai (白 芬)[1],*, Qingpu Wang (王青圃)[2], Zhaojun Liu (刘兆军)[2],
Zhiyong Jiao (焦志勇)[1], Xianfeng Xu (徐先锋)[1], and Hui Zhang (张 会)[1]

[1]*College of Science, China University of Petroleum (East China), Qingdao 266580, China*
[2]*School of Information Science & Engineering and Shandong Provincial Key Laboratory of Laser Technology*
and Application, Shandong University, Jinan 250100, China
*Corresponding author: baifen@upc.edu.cn

Two types of acousto-optically Q-switched Nd:YVO$_4$/KTA singly resonated optical parametric oscillators are performed. One is signal resonant, where a 1.5 μm wave resonates while a 3.5 μm wave does not. The other is idler resonant, where a 3.5 μm wave resonates while a 1.5 μm wave does not. All the experimental elements are kept the same for these two schemes except for the coatings of the optical parametic oscillator cavity output coupler. For these two kinds of lasers, the output characteristics of the threshold, output power, pulse width, peak power, and beam quality are measured and compared.

OCIS codes: 140.3460, 190.4970, 140.3540.
doi: 10.3788/COL201614.071402.

The wavelength conversion of laser beams in optical parametric oscillators (OPOs) is an effective method to generate tunable radiation as well as radiation at wavelengths outside the range of available laser materials[1–4]. If some upper frequency (ω_3), also known as the pump, is incident on a non-linear medium, then two frequencies (ω_1 and ω_2) will be produced according to the phase-matching principle and the energy conservation law ($\omega_3 = \omega_1 + \omega_2$)[5–8]. When both ω_1 and ω_2 are resonated, it is called a doubly resonant oscillator. If the system operates with either ω_1 or ω_2 resonated, it is called a singly resonant oscillator (SRO). As defined traditionally, the generated two waves from the SRO are called signal and idler waves for the high and low frequency ones, respectively. SROs possess the advantages of stable operation and easy coating, and hence have been extensively studied for forty years[4–6,9–19]. However, those studies conducted with SROs raise a question. For the generated two frequencies, which should be selected to resonate, the signal or the idler?

Here, we will address this question using KTA-SRO as an example. As one of the isomorphs of KTP, KTA possesses excellent characteristics, such as large non-linear coefficient, low temperature sensitivity, higher optical damage threshold, and wide transparency range (0.35–5.3 μm)[20,21]. Moreover, the ability to operate with non-critical phase matching (NCPM) is also an important advantage. NCPM has the advantages of no walk-off and a large acceptance angle[10]. It has been widely employed in OPOs based on KTP and its isomorphs for efficient parametric conversions. More recently, Duan's group investigated several RTP (RbTiOPO$_4$)-based OPOs by making full use of an NCPM scheme[22–24]. Employing the mature 1 μm laser as the pump source and utilizing the type II NCPM scheme, a KTA-OPO can generate 1.5 μm eye-safe and 3.5 μm mid-infrared lasers simultaneously. As

mentioned above, we denote the 1.5 μm wave as the signal and the 3.5 μm wave as the idler in this Letter. In past decades, KTA-OPOs driven by Q-switched Nd-doped laser sources (Nd:YALO, Nd:YAG, Nd:YVO$_4$, Nd:GdVO$_4$, etc.) have been widely used to generate 1.5 μm and (or) 3.5 μm waves with singly resonated configurations. The KTA-SRO in Refs. [11–17,25,26] operated with the signal radiation (1.5 μm) resonated. In Ref. [27], we reported the first idler-resonant KTA SRO. Driven by a Q-switched Nd:YAG laser, this KTA OPO operated with 3.5 μm radiation resonated, and a total output power of 825 mW was obtained. However, the complete comparison between the signal-resonant and idler-resonant KTA-SROs has seldom been investigated.

In this Letter, we prepare two types of diode end-pumped acousto-optical (AO) Q-switched Nd:YVO$_4$/KTA SROs. One is signal resonant, termed as Scheme 1, where the 1.5 μm wave resonates while the 3.5 μm wave does not. The other is idler resonant, termed as Scheme 2, where the 3.5 μm wave resonates while the 1.5 μm wave does not. In order to make a more accurate comparison, all the experimental elements were kept the same for these two schemes except for the coatings of the OPO cavity output coupler (OC). Comparative studies on the threshold, output power, peak power, pulse width, and beam quality are performed. When weighing the benefits of these two schemes, we consider both the advantages and disadvantages of each. For the signal-resonant scheme (Scheme 1), the KTA-SRO has the advantage of a lower threshold and higher output power, but presents the disadvantage of poor beam quality for the 3.5 μm laser. Conversely, the idler-resonant KTA-SRO (Scheme 2) achieves significantly improved beam quality for the 3.5 μm laser, but the threshold is high and the output power is relatively low. However, no matter whether the 1.5 μm wave resonates or the 3.5 μm

wave resonates, the results show that in an SRO, the resonant radiation has better beam quality but a wider pulse width than the non-resonant radiation.

Figure 1 represents the experimental setup for two types of KTA-SROs. The cavity was carefully designed as a straight intracavity OPO configuration. The fundamental wave oscillates in a convex-plano cavity, and inside it is the plano–plano OPO cavity. A fiber-coupled CW LD (NA = 0.22, $d_{core} = 600$ μm) was used as the pumping source. A focusing lens system with a focal length of 50 mm and a coupling efficiency of 95% is used to re-image the pump beam into the laser crystal. The focused beam diameter was 600 μm after the focusing lens system. Here, a ceramic Nd:YVO$_4$ crystal (0.3 at. % Nd-doped, 3 mm × 3 mm × 10 mm) was used as the gain medium. Both surfaces of Nd:YVO$_4$ were anti-reflection (AR) coated at 808 and 1064 nm ($R < 0.2$%). The KTA crystal (4 mm × 4 mm × 25 mm) was cut along its X-axis ($\theta = 90°$, $\phi = 0°$) to realize type II non-critical-phase-matching. Its coating were AR ($R < 0.2$%) at 1064 and 1535 nm and high-transmission (HT) ($T > 95$%) at 3470 nm on both surfaces. The Nd:YVO$_4$ and KTA crystals were wrapped with indium foil and mounted in water-cooled copper blocks. The water temperature was maintained at 20°C. The 38 mm-long AO Q-switch (Gooch and Housego) had AR coatings ($R < 0.2$%) on both faces at 1064 nm and was driven at a 41 MHz center frequency with 15 W of radio frequency power. The rear mirror (RM) was a 500 mm radius-of-curvature plano-convex mirror. The entrance face of the RM was coated for AR at 808 nm ($R < 0.2$%). The other face was coated for high reflection (HR) at 1064 nm ($R > 99.8$%) and HT at 808 nm ($T > 99$%). M1 was made of infrared silica glass (JGS3). Its one surface was coated for AR at 1064 nm ($R < 0.2$%), and the other surface coated for HT at 1064 nm ($T > 99.5$%) and HR at both 1535 and 3470 nm ($R > 99.8$%). All the experimental elements were kept the same for these two types of OPOs except for the coatings of OC. The overall cavity length was 93 mm and the OPO cavity length was 31 mm for both schemes.

For the signal-resonant KTA-SRO (Scheme 1), we used a flat mirror made of CaF$_2$ as the OC (OC1). OC1 was coated for HR at 1064 nm ($R > 99.9$%), partial reflection (PR) at 1535 nm ($R = 80$%), and HT at 3470 nm ($T > 95$%). Here, the 1.5 μm wave resonated, while the

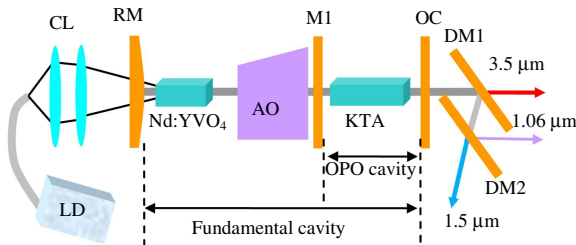3.5 μm wave did not. Thus, the resonator was a singly resonated OPO with a 1.5 μm wave oscillating between M1 and OC1. The generated 3.5 μm laser transmitting in the forward direction can output directly. The 3.5 μm laser transmitting in the backward direction would be reflected by M1 and finally output through OC1. As a result, we could collect the generated 3.5 μm laser in both directions.

For the idler-resonant KTA-SRO (Scheme 2), a flat mirror made of Al$_2$O$_3$ was employed as the OC (OC2). OC2 was coated for HR at 1064 nm ($R > 99.9$%), PR at 3470 nm ($R = 91$%), and HT at 1535 nm ($T > 99.3$%). Thus, the resonator was an idler-resonated OPO with a 3.5 μm wave oscillating between M1 and OC1. Also, the generated 1.5 μm laser in both directions could be output through OC2.

An OPO can only operate above the oscillating threshold, so the pump radiation must be intensive enough to reach the threshold. Before studying the OPO characteristics, an OC with a PR coating ($R = 90$%) at 1064 nm was used to investigate the performance of the fundamental laser. The KTA crystal and M1 were placed inside the laser cavity without the OPO functioning. Figure 2 shows the output power of 1064 nm laser at conditions of continuous-wave operation and Q-switching operation with pulse repetition rates (PRRs) of 40, 50, and 60 kHz. It can been seen that with the diode pump power increasing from 18.1 to 26.4 W, the output power of the 1064 nm monotonic laser increased. Under an LD pump power of 26.4 W and a PRR of 40 kHz, the output power of the fundamental laser obtained was 8.6 W. The conversion efficiency from the LD pump power to the 1064 nm laser was 33.2%.

Then, using the OCs designed for OPO operation, we studied the output characteristics, including the threshold, output power, pulse width, peak power, and beam quality for these two types of OPOs. Table 1 gives the threshold results at PRRs of 40, 50, and 60 kHz. It can be seen that the threshold for the idler-resonant OPO
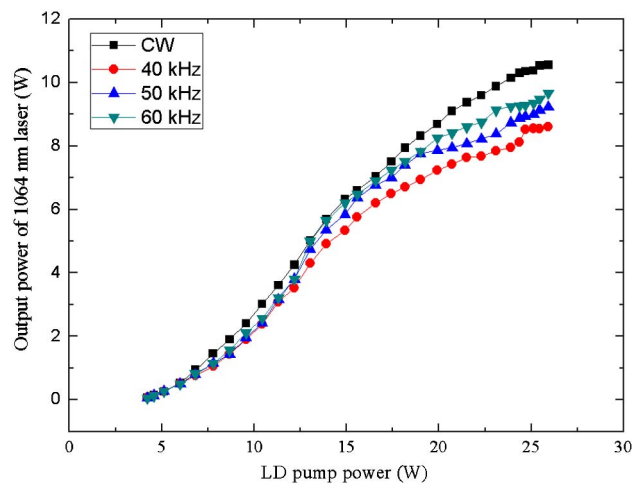

Fig. 1. Experimental setup for Nd:YVO$_4$/KTA SRO. CL, coupling lens; AO, acousto-optic Q-switch; DM, dichroic mirror.

Fig. 2. Average output powers of 1064 nm laser with respect to the diode pump powers.

Table 1. Threshold at Different PRRs for Two Types of KTA-SROs

	40 kHz	50 kHz	60 kHz
Signal-resonant SRO	10.03 W	11.28 W	13.33 W
Idler-resonant SRO	15.58 W	16.58 W	19.92 W

was much higher than that of the signal-resonant OPO. For example, the values were measured to be 15.58 W for the idler-resonant OPO, which was 1.6 times greater than that of the signal-resonant OPO (10.03 W). In addition, the threshold increased as the PRR increasing. That was because at a lower PRR, the stored energy during one pump period was high enough that the threshold could be reached more easily.

When measuring the output power characteristic, two dichroic mirrors (DMs) were used to separate the fundamental, signal, and idler powers. DM1 was made of CaF_2 and coated for HT at 3470 nm ($T > 99\%$) and HR at both 1535 and 1064 nm ($R > 99.5\%$). DM2 was made of BK7 and coated for HT at 1535 nm ($T > 99.5\%$) and HR at 1064 nm ($R > 99.8\%$). All laser powers were measured with an EPM2000 power meter (Coherent Inc.). Figure 3 depicts the average output powers at 40 kHz for both Scheme 1 and Scheme 2. We distinguish the results for Scheme 1 and Scheme 2 in red and blue. The dots and triangles correspond to the results for the 1.5 and 3.5 μm lasers, respectively. For Scheme 1, the highest 1.5 and 3.5 μm powers obtained were 2.03 and 753 mW, respectively, at a pump power of 24.7 W. The conversion efficiency from the LD pump power to the total OPO lasers was 11.3%.The output powers saturated and declined when the pump power was higher than 24.5 W. For Scheme 2, the highest signal and idler powers were 1.69 W and 214 mW, respectively, which were obtained at a pump power of 26.4 W. The conversion efficiency from the LD pump power to the total OPO lasers was 7.2%.
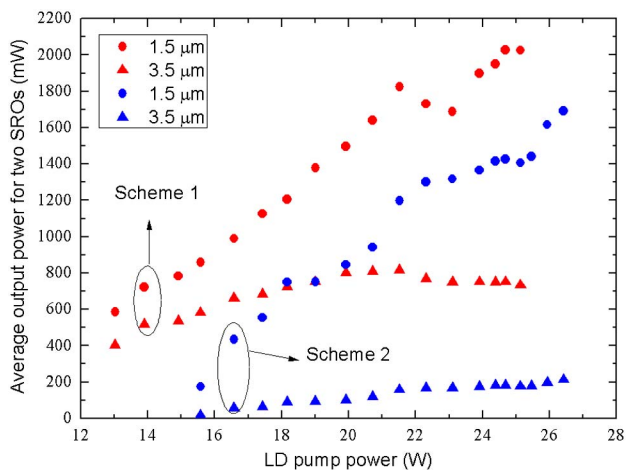

Fig. 3. Average output powers with respect to the diode pump powers for signal and idler-resonant KTA-SROs.

Limited by the LD power, we did not try a higher pumping power. Also, we did not observe damage to either the coatings or the crystals.

From this figure, we can see that the output power from Scheme 2 is relatively low (about 60% of the total power from Scheme 1). That means the conversion efficiency from the LD pump power to the OPO laser power was much lower for Scheme 2. Although both of the OCs were coated for HR at 1064 nm ($R > 99.9\%$), the fundamental laser could be coupled out of the cavity due to the high intracavity power density. We measured the 1064 nm laser power after the OCs for both OPOs. The result for Scheme 1 was less than 10 mW, and for Scheme 2, it was about 500 mW. Higher coupled-out power resulted from a higher density inside the cavity for the 1064 nm laser in Scheme 2. This means the efficiency from the fundamental laser to the OPO was lower for Scheme 2, which also can explain the lower efficiency from the LD pump power to the OPO for Scheme 2. The more fundamental photons failed to convert during the interaction, the more the 1064 nm laser was residual, and then the intracavity density could be higher. As a result, a higher output of 1064 nm power was obtained for Scheme 2. Addtionally, in both Scheme 1 and Scheme 2, the output power of the 1.5 μm laser was always higher than that of the 3.5 μm laser. This was mainly because of the lower quantum defect of 1.5 μm radiation.

The output power stability of Scheme 1 was measured to be better than 1% within ten minutes during the operation, and that of Scheme 2 was about 3% during the operation. The worse stability of Scheme 2 was mainly because of the more serious thermal effects from the lower conversion efficiency.

We studied the time characteristics of the two types of OPOs by using a digital phosphor oscilloscope (TDS 5052B, Tektronix). The 1.5 μm pulses were detected by an InGaAs photodiode, and the 3.5 μm pulses were detected by an HgCdZnTe photoconductive detector. We measured the response parameter with a CW mode-locked 1064 nm laser, which had a pulse width of around 40 ps. The result for the InGaAs case was around 1 ns, and that of HgCdZnTe case was around 5 ns. The pulse widths (FWHM) at 40 kHz for Schemes 1 and 2 are shown in Fig. 4. It is noted that the pulse width results in Fig. 4 were obtained from the deconvolution of the recorded pulse shape and the equipment response function. Each point was obtained by averaging ten arbitrary experimental values. It was obvious that in Scheme 1, the pulse widths of the 1.5 μm laser were wider than those of the 3.5 μm laser, whereas it was the opposite in Scheme 2. That is to say, in SROs, the pulse width of the non-resonated one is shorter than that of the other. Because the OPO is a threshold process, the signal and idler light are only produced when the fundamental wave is intense enough. Starting the OPO quickly results in a strong depletion of the pump field. As a result, the pulse widths of the signal and idler were far shorter than that of the fundamental wave. If the remaining fundamental energy
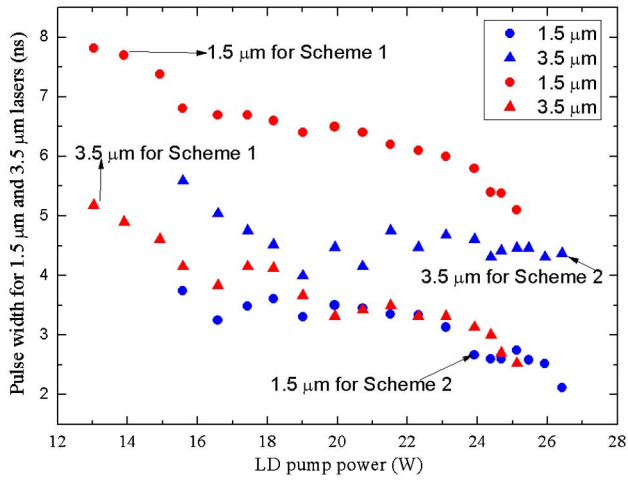
Fig. 4. Pulse widths with respect to the diode pump powers for two types of KTA-SROs.

Fig. 6. Peak powers with respect to the diode pump powers for two types of KTA-SROs.

is sufficient to permit the repetition of the process, the second signal and idler pulse could build up. This pulse-series phenomenon was observed in our experiment with Scheme 2. Taking the case of the pump power of 24.7 W as an example, we give the typical pulse shapes recorded from the oscilloscope in Fig. 5, where Figs. 5(a) and 5(b) are the results for Scheme 1 and 2, respectively.

Figure 6 shows the peak power for these KTA-SROs. From Fig. 6, we can see that the peak power of the 1.5 μm wave in Scheme 2 was obtained to be 20 kW at a pump power of 26.4 W, which was the highest value in the two experiments. This was attributed to the narrow pulse width of the 1.5 μm laser in Scheme 2.

The output beam profiles were monitored by a Nanoscan beam analyzer and a precision linear stage (Zolix, Inc). By focusing the beam with a ZnSe lens ($f = 100$ mm), we
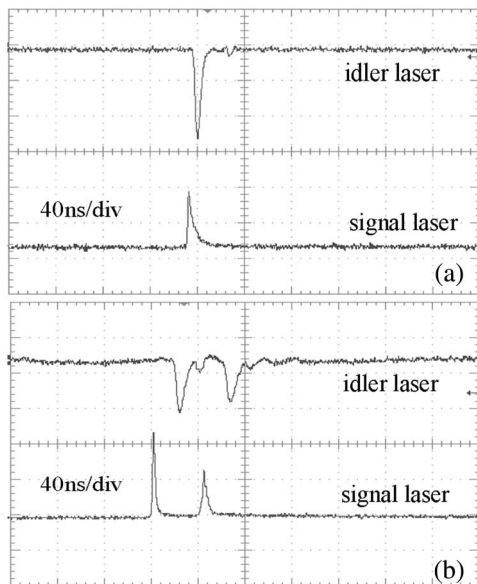
measured the beam quality factors (M^2) of the 1.5 and 3.5 μm waves for both Schemes 1 and 2 at the pump power of 24.7 W and 40 kHz. The values are shown in Table 2. It is seen that in the signal-resonant KTA OPO, the beam quality for the 1.5 μm laser was better, while in the idler-resonant KTA OPO, the beam quality of the 3.5 μm laser was significantly improved compared with signal-resonant OPO. That is to say, for each scheme, the beam quality of the resonant laser is always better than that of the other. For the SRO, it can be considered that the non-resonant wave does not experience any resonator. Thus, the generated wave is free to propagate along the axis and can be directly output without restriction. The resonant one propagates originally with several cavity eigenmodes. With the light oscillating, the fraction with higher-order modes is gradually lost from the edges of the gain region by diffraction. After a few round trips of the cavity, the fraction with lower-order modes remains. This restriction results in a good beam quality for the resonated light.

In conclusion, we realize two types of diode-end pumped AO Q-switched Nd:YVO$_4$/KTA SROs. A complete comparison of the output performances between the signal-resonant and idler-resonant KTA-SROs is studied. With a diode pump power of 24.7 W, the signal-resonant scheme generates an average 1.5 μm power of 2.03 W and an average 3.5 μm power of 753 mW. The idler-resonant scheme

Fig. 5. Typical pulse shapes for two types of KTA-SRO: (a) signal resonant and (b) idler resonant.

Table 2. Beam Quality Factors for Two Types of KTA-SROs

	1.5 μm wave		3.5 μm wave	
	Horizontal	Vertical	Horizontal	Vertical
Signal-resonant SRO	1.5 ± 0.1	1.6 ± 0.1	7.3 ± 0.1	8.0 ± 0.1
Idler-resonant KTA-SRO	4.9 ± 0.1	5.1 ± 0.1	2.2 ± 0.1	3.2 ± 0.1

produces an average power of 1.69 W at 1.5 μm and an average power of 214 mW at 3.5 μm. Moreover, the signal-resonant OPO has a lower threshold, and the highest peak power of the 1.5 μm laser is obtained in the idler-resonant KTA-SRO. Nevertheless, from the mid-infrared application viewpoint, the idler-resonant scheme provides better beam quality for the 3.5 μm output beams.

References

1. K. L. Vodopyanov, F. Ganikhanov, J. P. Maffetone, I. Zwieback, and W. Ruderman, Opt. Lett. **25**, 841 (2000).
2. U. Strößner, J.-P. Meyn, R. Wallenstein, P. Urenski, A. Arie, G. Rosenman, J. Mlynek, and S. Schiller, J. Opt. Soc. Am. B **19**, 1419 (2002).
3. L. E. Myers, R. C. Eckardt, M. M. Fejer, R. L. Byer, W. R. Bosenberg, and J. W. Pierce, J. Opt. Soc. Am. B **12**, 2102 (1995).
4. W. Żendzian, J. K. Jabczyńsk, and J. Kwiatkowski, Appl. Phys. B **76**, 355 (2003).
5. T. Debuisschert, J. Raffy, J.-P. Pocholle, and M. Papuchon, J. Opt. Soc. Am. B **13**, 1569 (1996).
6. J. Falk, J. M. Yarborough, and E. O. Ammann, IEEE J. Quantum Electron **7**, 359 (1971).
7. H. Li, X. Zhu, X. Ma, S. Li, and A. Chen, Chin. Opt. Lett. **13**, 111402 (2015).
8. H. Li, X. Zhu, X. Ma, S. Li, C. Huang, J. Zhang, and W. Chen, Chin. Opt. Lett. **12**, 91401 (2014).
9. Y. F. Chen, S. W. Chen, L. Y. Tsai, Y. C. Chen, and C. H. Chien, Appl. Phys. B **79**, 823 (2004).
10. G. A. Rines, D. M. Rines, and P. F. Moulton, Adv. Solid State Lasers **20**, 461 (1994).
11. Z. J. Liu, Q. P. Wang, X. Y. Zhang, Z. J. Liu, H. Wang, J. Chang, S. Z. Fan, W. J. Sun, G. F. Jin, X. T. Tao, S. J. Zhang, and H. J. Zhang, Appl. Phys. B **92**, 37 (2008).
12. H. Y. Zhu, G. Zhang, H. B. Chen, C. H. Huang, Y. Wei, Y. M. Duan, Y. D. Huang, H. Y. Wang, and G. Qiu, Opt. Express **17**, 20669 (2009).
13. R. F. Wu, K. S. Lai, H. Wong, W.-J. Xie, Y. Lim, and E. Lau, Opt. Express **8**, 694 (2001).
14. X. L. Dong, B. T. Zhang, J. L. He, H. T. Huang, K. J. Yang, J. L. Xu, C. H. Zuo, S. Zhao, G. Qiu, and Z. K. Liu, Opt. Commun. **282**, 1668 (2009).
15. J. G. Miao, J. Y. Peng, B. S. Wang, and H. M. Tan, Appl. Opt. **47**, 4287 (2008).
16. F. Bai, Q. P. Wang, Z. J. Liu, X. Y. Zhang, X. B. Wan, W. X. Lan, G. F. Jin, X. T. Tao, and Y. X. Sun, Opt. Express **20**, 807 (2012).
17. K. Zhong, J. Q. Yao, D. G. Xu, J. L. Wang, J. S. Li, and P. Wang, Appl. Phys. B **100**, 749 (2010).
18. S. French, A. Miller, and M. Ebrahimzadeh, Opt. Quantum Electron. **29**, 999 (1997).
19. W. J. Sun, Q. P. Wang, Z. J. Liu, X. Y. Zhang, F. Bai, X. B. Wan, G. F. Jin, X. T. Tao, and Y. X. Sun, Appl. Phys. B **104**, 87 (2011).
20. J. D. Bierlein, H. Vanherzeele, and A. A. Ballman, Appl. Phys. Lett. **54**, 783 (1989).
21. G. M. Loiacono, D. N. Loiacono, J. J. Zola, R. A. Stolzenberger, T. McGee, and R. G. Norwood, Appl. Phys. Lett. **61**, 895 (1992).
22. Y. Duan, H. Zhu, Y. Ye, D. Zhang, G. Zhang, and D. Tang, Opt. Lett. **39**, 1314 (2014).
23. H. Y. Zhu, Y. M. Duan, H. Y. Wang, Z. H. Shao, Y. J. Zhang, G. Zhang, J. Zhang, and D. Y. Tang, IEEE J. Sel. Top. Quantum Electron. **21**, 173 (2015).
24. Y. Duan, H. Zhu, H. Wang, P. Wei, C. Zheng, and Y. Zhang, IEEE Photon. Technol. Lett. **27**, 359 (2015).
25. K. Zhong, J. S. Li, H. X. Cui, Y. Y. W. D. G. Xu, R. Zhou, J. L. Wang, P. Wang, and J. Q. Yao, Chin. Phys. Lett. **26**, 049401 (2009).
26. Q. B. Sun, H. J. Liu, N. Huang, C. Ruan, S. L. Zhu, and W. Zhao, Laser Phys. Lett. **8**, 16 (2011).
27. F. Bai, Q. Wang, Z. Liu, X. Zhang, W. Lan, X. Tao, and Y. Sun, Appl. Phys. B **112**, 83 (2013).